EXPERIMENTAL EVALUATION OF FLOW DISTORTION AT TILT-ROTOR FULL-SCALE MODEL AIR INTAKE WIND TUNNEL TEST

Remco Habing, remco.habing@nlr.nl, Netherlands Aerospace Centre (NL)

Iwan Philipsen, iwan.philipsen@dnw.aero, German-Dutch Wind Tunnels (NL)

Matthias Müller, m.mueller@deharde.de, Deharde (DE)

Matteo Pecoraro, matteo.pecoraro@leonardocompany.com, Leonardo Helicopters (IT)

Abstract

Within the Clean Sky 2 Fast Rotorcraft platform, a Next Generation Civil Tilt-Rotor demonstrator is being developed. Within the related TRINIDAT project the key driving aerodynamic choices of the engine air intake configuration are being investigated. A wind tunnel model has been successfully designed and manufactured for full-scale intake testing of the basic intake configuration. The model is comprised of a nacelle, modular intake duct, rotatable spinner hub (rotor head) and wing part including deflectable aileron. In order to assess the flow quality at the Air Inlet Plane (AIP), a novel highly instrumented rotary rake has been designed. The model also includes a large amount of static pressure taps on wing and intake duct surfaces. A wind tunnel test in the DNW-LLF has been successfully performed, simulating the full flight envelope and parameter variations. The adopted scaling methodology is explained. The 6 x 6 m^2 test section allowed to test the full-scale model at $Ma = 0.40$ which is nearly cruise Mach number. The test program included a wide range of variations in angle of attack, sideslip angle, aileron deflection and suction mass-flow rate. Post-processing of the test data yielded a large database including flow distortion parameters based on the total pressure field and the velocity field in the AIP. The sensitivity of key distortion parameters to variation of model attitude, aileron deflection and mass-flow rate has been obtained for a selected set of conditions. The development of unsteady pressures along the intake duct including AIP has been characterized as well.

1. INTRODUCTION

Within the Clean Sky 2 Fast Rotorcraft platform, a Next Generation Civil Tilt-Rotor (NGCTR) demonstrator is being developed [1] (Fig. 1). The NGCTR concept is a next step in the development of a European civil tilt-rotor, following the earlier work on the AW609 concept and the ERICA concept [4]. The main benefit of the NGCTR configuration (compared to helicopter and turboprop) is that it offers reduced travel time on short and medium distances up to 500 nautical miles (approx. 1000 km). For NGCTR, to reduce system complexity and weight, it has been decided to keep the engine at fixed pitch angle setting and make only the spinner and rotor rotatable. This change of engine integration architecture requires research to assure a good flow quality in the engine intake ducts under all flying conditions, with a focus on high efficiency in aircraft mode and safe and proper operation in other flight modes.

The related TRINIDAT project [2] has two main objectives, viz. i) to assess, by dedicated experiments and advanced CFD analysis, the key driving aerodynamic choices of the intakes configuration, and ii) to investigate the icing and snow effects on the intakes, providing early input for ice protection system development and certification [13]. The first objective includes a basic as well as an optimized intake duct. The present paper summarizes results of the TRINIDAT project, related to model design, test simulation methodology, test procedure and analysis results obtained from the conducted wind tunnel test with the basic intake configuration.

Fig. 1 Artist view of NGCTR concept in cruise condition

Presented at 47th European Rotorcraft Forum, United Kingdom, 7-9th September, 2021

2. WIND TUNNEL MODEL

2.1. Model design & manufacturing

The model is comprised of a nacelle, modular intake duct, rotatable spinner hub (rotor head) and wing part including deflectable aileron (Fig. 2). The model represents a full-scale air intake excluding rotor. As for the NGCTR aircraft both rotors will rotate symmetrically, a half-model configuration is considered. The model assembly is basically comprised of three parts, i.e. nacelle, wing and wind tunnel model support. In order to be able to capture high loads an overlap of the steel wing bottom plate with the aluminium wing was realized. The wing contains cable holes and a sealed wing box with rounded suction hole. A provision for future testing of vortex generators also has been realized. A trade-off between truncated wing span and allowance of sideslip settings (-10 to 10 deg) has been designed.

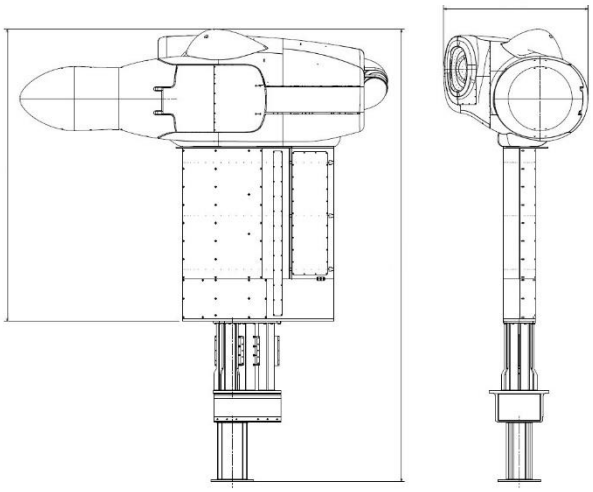

Fig. 2 Design of full-scale wind tunnel model

Due to the tilting rotor head concept of the NGCTR, the intake duct changes from an elliptical cross-section to an annular cross-section of the Air Intake Plane (AIP) for the engine (Fig. 3). In order to assess the flow quality at the AIP annulus, two key elements were addressed. First, an internal piping system is designed to allow for generating the proper suction mass flow-rate at the AIP. Second, a specially designed rotary rake is mounted at the AIP to allow for accurately measuring the flow quality (Fig. 4). The suction pipe is designed to have sufficient axial length from AIP to first bending section to neglect the downstream flow curvature effect on the AIP.

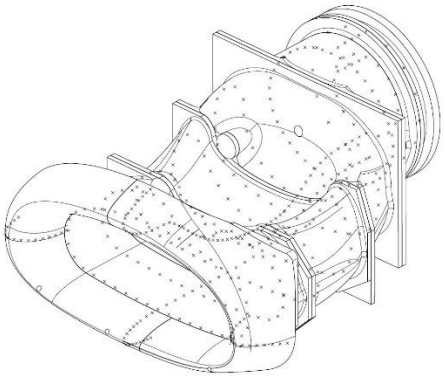

Fig. 3 Design of basic intake model and pressure tap distribution

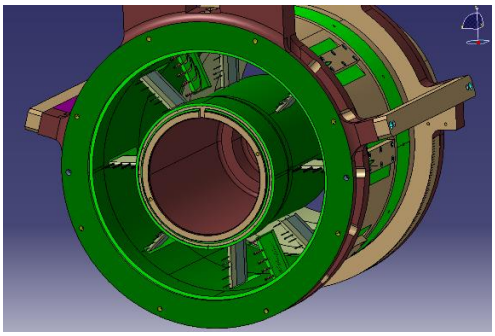

Fig. 4 Design of novel rotary rake and instrumentation at AIP

2.2. Remote controls & instrumentation

The model is comprised of three remote control systems, i.e. for aileron deflection (-30 to 70 deg, trailing edge down is positive), rotor hub pitch angle (0 to 90 deg) and rotary rake settings (-90 to 90 deg). The system drives are servo motors with adjustable gearing, flex coupling and include absolute encoders (position sensors) which have been calibrated. The limit switches design ensures the above mentioned full range angular settings.

The highly instrumented rotary rake (Fig. 5) consists of 40 steady total pressure probes (8 equiangularly spaced rakes with 5 area-weighed radially positioned probes per rake, following SAE [3]), 10 unsteady total pressure sensors (2 dedicated rakes with co-annular design [5] for steady and unsteady total pressure), 6 total temperature sensors (integrated in pressure rakes) and 10 flow-directional probes (2 rakes, 180 deg spaced, with 5 area-weighed radially positioned 5-hole probes per rake), while keeping a very low flow blockage of 0.3% (compare e.g. Ref. [5]). The flow-directional probe rakes have been calibrated in NLR's AWT prior to WT testing.

The model also includes a large amount of static pressure taps (on 3 wing sections at different spanwise positions crossing the aileron (168

Presented at 47th European Rotorcraft Forum, United Kingdom, 7-9th September, 2021

taps), intake lip and duct (366 taps, Fig. 3) and AIP annular surfaces (32 taps, Fig. 5)). The intake lip contains 4 streamwise tap sections, while the intake duct contains 2 streamwise tap sections and 6 circumferential tap sections (excl. AIP). The intake duct also includes 10 unsteady static pressure sensors.

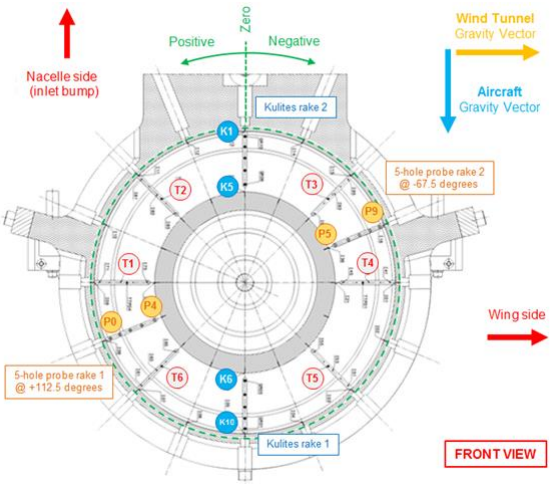

Fig. 5 Design of instrumentation layout at AIP

3. WIND TUNNEL TEST

3.1. Simulation and test conditions

Free flight conditions have been specified by Leonardo Helicopters, mainly as guidelines for the CFD simulations and covering the full flight envelope. The translation from flight- to wind tunnel test conditions is performed by application of similarity rules. The applied rules consider both the inverse capture ratio (ICR) as well as the Reynolds number (Re_{AIP}) based on bulk flow conditions at the AIP to remain constant. It can then be shown that for full-scale testing the following relation for the freestream wind tunnel velocity holds:

$$(1) \qquad V_{WT} = \frac{\rho_{Flight}}{\rho_{WT}} \frac{\mu_{AIP,WT}}{\mu_{AIP,Flight}} V_{Flight}$$

Applying Sutherland's law for dynamic viscosity, this relation contains a coefficient that strongly depends on air density and a coefficient that weakly depends on static temperature in the AIP. In general these equations need to be solved iteratively. However, it can be shown that for low Mach number in the AIP ($Ma_{AIP} < Ma < 0.4$) the static temperature in the AIP is with good approximation (≤ 3%) equal to the freestream static temperature. As iterative methods in online processing are not recommended, above approximation is employed in the translation procedure. From eq. (1) it is recognized that simulating high altitude conditions in a wind tunnel require significant reduction in wind tunnel speed (compared to free flight). It can be shown that for the Re_{AIP} similitude only a limited increase in mass flow rate is required.

As the test is performed without rotor blades, the rotor induced wind field in flight condition has been obtained from application of Glauert's rotor flow model [6]. Knowing that the rotor radius R is much larger than the air intake dimensions, it is recognized that the intake is always in the flow field generated by the rotor, for all flight modes. The rotor induced wind field v_i (i.e. rotor generated axial velocity) is obtained in an iterative procedure from the following equation:

$$(2) \qquad v_i^4 + 2Vv_i^3 \cos(\theta_r + \alpha) + v_i^2 V^2 = \frac{T^2}{4\rho^2\pi^2R^4}$$

where θ_r is the rotor hub pitch angle, α is the angle of attack, T is the rotor thrust. It is noted that from eq. (2) well-known limit case equations can be obtained for small induced velocities in airplane mode ($\frac{v_i}{V} \ll 1$) or significant induced velocities in hover mode ($V = 0$). With the rotor induced velocity component directed along the rotor axis, and assuming the effective total velocity magnitude and direction for the intake is the same as in the rotor plane, it is possible to derive expressions for the effective flight velocity and effective angle of attack:

$$(3) \quad V_{e,Flight} = \sqrt{[V\cos(\theta_r + \alpha) + v_i]^2 + [V\sin(\theta_r + \alpha)]^2}$$

$$(4) \qquad \alpha_{e,Flight} = \alpha - atan\left[\frac{v_i \sin(\alpha+\theta_r)}{V + v_i \cos(\alpha+\theta_r)}\right]$$

For cruise conditions a trivial solution is obtained ($V_{e,Flight} = V$ and $\alpha_{e,Flight} = \alpha$). For hover conditions these result in $V_{e,Flight} = v_i$ and $\alpha_{e,Flight} = -\theta_r$. For conversion modes these equations are of particular interest.

3.2. Test setup

The Large-Low-Speed-Facility (LLF) of DNW is an atmospheric, single return wind tunnel with three exchangeable closed test section arrangements (Fig. 6). The LLF can also be operated in an open-jet mode. The measurements with the

Presented at 47th European Rotorcraft Forum, United Kingdom, 7-9th September, 2021

TRINIDAT full-scale intake model are performed in the 6 x 6 m^2 test section (airplane mode and conversion modes) and 8 x 6 m^2 test section for the VTOL mode. The 6 x 6 m^2 test section allowed to test the full-scale model at $Ma = 0.40$ which is nearly cruise Mach number.

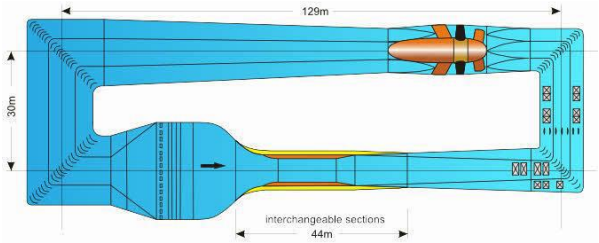

Fig. 6 Airline and dimensions of the LLF (top view)

The model is mounted on a turntable in the test section floor (which allows angle of attack variation), with direct interfacing to the alpha-mechanism (cradle) inside the turntable (allowing combined sideslip variation), see Fig. 7. The spinner hub axis at 0 deg pitch is located at tunnel centre line.

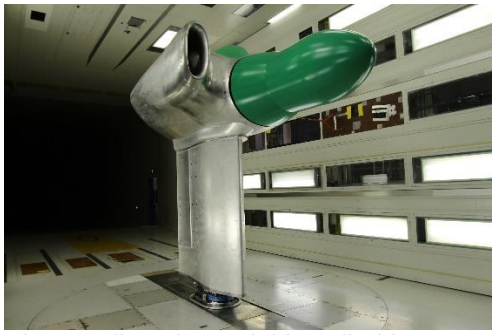
Fig. 7 Full-scale model installed in DNW-LLF wind tunnel test section

Applying homogeneous transformations yields the model geometrical setting angles from combined aerodynamic angle of attack and sideslip angle.

The model is interfaced with a suction system located underneath the test section. This system consists of a piping and measurement system with 4 Roots Blowers, which are capable to attain the maximum required mass-flow rate of 6.9 kg/s through the inlet of the intake model. The Roots Blowers are calibrated prior to testing.

3.3. Instrumentation & data acquisition

The standard wind tunnel reference system is calibrated prior to testing and used to obtain the freestream flow quantities. In addition six wall pressure tap strips are applied on the test section walls to allow for model overall blockage correction. The model related instrumentation includes measurement of model incidence and roll angle, steady pressures, unsteady pressures, temperatures and position of remote controls.

All data is acquired in step and pause mode. In order to meet the SAE requirements [3], the integration time was set to 30 s per data point (after reaching a stable test condition). The Static Data Acquisition system samples the data at a rate of 20 Hz (with LPF = 3 Hz) and stores the averaged value incl. statistics. The Dynamic Data Acquisition system is used to acquire the time signals of the unsteady pressure sensors. Following the guidelines of SAE [3], taking into account sources of unsteadiness such as freestream turbulence and possible flow separation at intake duct, a sampling rate of 12.8 kHz during 30 s is used.

3.4. Test program & procedure

The test program includes full flight conditions, high-speed conditions and parameter variations (angle of attack, sideslip, aileron deflection, mass-flow rate) for airplane mode (AP), conversion modes (CM, rotor hub pitch 30, 50, 75 deg) and VTOL mode. The conducted test matrix included a wide variety of model attitude (i.e. rotor hub pitch [0, 90], effective angle of attack [-90, 37], sideslip [-10, 10], aileron [-30, 70], all in deg).

The following test procedure was applied for setting the flow conditions. The test matrix contained estimations of the required mass-flow rate and freestream velocity, based on the adapted scaling methodology (see 3.1). First, the required Reynolds number was set by control of the mass-flow rate W_{WT}, see eq. (5). Then the inverse capture ratio was set by control of the freestream velocity V_{WT} subsequently, see eq. (6).

(5) $$Re_{AIP} = \frac{(W_{WT}/A_{AIP})}{\mu_{WT}} D_{h,AIP}$$

(6) $$ICR = \frac{\rho_{WT} V_{WT}}{(W_{WT}/A_{AIP})}$$

These scaling parameters have following required values for the full flight conditions: $3.4\text{E}5 \leq Re_{AIP} \leq 6.7\text{E}5$ and $0.3 \leq ICR \leq 1.8$.

The spatial resolution of the flow measurements in the AIP has been increased by using the rotary rake. The test matrix contained 4 types of settings, i.e.

- [0] deg, fixed rake, mean Pt field
- [45, 67.5, 90] deg, rotating rake, refined mean Pt field (and swirl in top/bottom sector)

Presented at 47th European Rotorcraft Forum, United Kingdom, 7-9th September, 2021

- [45 (7.5) 90] deg, rotating rake, extra refined mean Pt field (and swirl in top/bottom sector)
- [-90 (15) 75] deg, rotating rake, full scan for complete flow field (incl. swirl and unsteady pressure)

Following the SAE regulations [3], in clockwise direction is considered positive for pilot view (i.e. upstream looking), see also Fig. 5.

Considering all test conditions, the static temperature in the AIP deviates on average 0.7% (and no more than 2.5%) from the freestream static temperature. This confirms an important assumption of the scaling methodology (3.1).

3.5. Data processing

The data processing system allows online and offline data processing, presentation and storage of measured data. A dedicated tool for online checking the intake- and wing performance has been developed, see Fig. 8. The final results are corrected for zero drift of the instrumentation and blockage of the wind tunnel model.

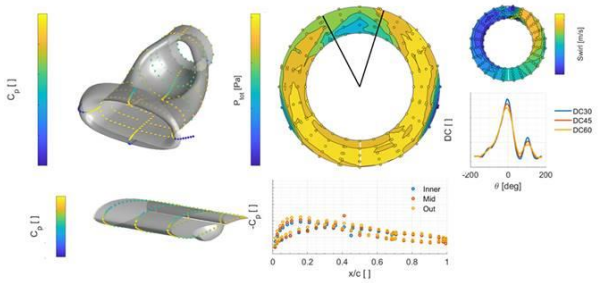

Fig. 8 Dedicated online monitoring tool

During the test execution online blockage correction was performed with the neo-classical corrections [8,9]. As the wind tunnel model is not equipped with a force balance, only corrections for solid blockage (wing, nacelle) and inlet blockage are considered.

The final test data was established by replacing the neo-classical corrections by an offline overall blockage correction based on a wall pressure signature method [10,11]. It is noted that the wind tunnel test entry with the optimized intake duct [2] is anticipated with an online blockage correction using the wall pressure method.

The final data have thus been corrected for wall induced flow blockage effects, which can be considerable for large angle of attack (for AP mode a typical value of 6% is found, while for VTOL mode typically 16% is found).

4. ANALYSIS OF TEST DATA

4.1. Flow distortion parameters

The importance of the effect of flow non-uniformities on an aeroengine has resulted in the development of a range of reduced-order parameters to quantify the level of distortion being presented to the engine [3,7]. The flow quality at the AIP of the basic intake model has been characterized by calculation of flow distortion parameters in dedicated MATLAB® scripts, taking the final test data as input. These parameters are largely based on the distribution of total pressure in the AIP.

The total pressure distortion at the AIP is quantified in terms of sectional distortion coefficient $DC60(\theta)$, circumferential distortion index CDI and radial distortion index RDI. $DC60(\theta)$ is defined by the difference between the area-averaged total pressure at the AIP $\overline{p0_{AIP}}$ and the average total pressure in a sector of 60 deg at circumferential mid-angle $\overline{p0_\theta}$ and is non-dimensionalized by the mean dynamic head of the whole AIP $\overline{q_{AIP}}$ as

$$(7) \qquad \mathrm{DC60}(\theta) = \frac{\overline{p0_{AIP}} - \overline{p0_\theta}}{\overline{q_{AIP}}}$$

At the maximum of the profile, two parameters are defined; $DC60MAX$ as maximum value and θ_{max} as related angular position. The CDI assesses the uniformity of the circumferential total pressure distribution at a specific radial position and is defined as

$$(8)\ \mathrm{CDI} = max_{i=1}^{4}\left(\frac{1}{2}\left[\frac{\overline{p0_i} - \min(p0)_i}{\overline{p0_{AIP}}} + \frac{\overline{p0_{i+1}} - \min(p0)_{i+1}}{\overline{p0_{AIP}}}\right]\right)$$

where $\overline{p0_i}$ is the average total pressure of the circumferential pressure distribution of the i^{th} ring (i=1..5) and $\min(p0)_i$ is the minimum total pressure along this same ring. Non-uniformities in the radial distortion are evaluated by the RDI which is defined as

$$(9) \qquad \mathrm{RDI} = max\left(\frac{\overline{p0_{AIP}} - \overline{p0}_{i=1}}{\overline{p0_{AIP}}}, \frac{\overline{p0_{AIP}} - \overline{p0}_{i=5}}{\overline{p0_{AIP}}}\right)$$

where $\overline{p0}_{i=1}$ is the average total pressure of the pressure distribution of the inner ring and $\overline{p0}_{i=5}$ is the average total pressure at the outer ring.

Additional metrics have been developed that consider total pressure distortion as a ring-based radial distribution of specific parameters, where radial and circumferential distortions are quantified separately. The circumferential total

Presented at 47th European Rotorcraft Forum, United Kingdom, 7-9th September, 2021

pressure distribution $p0$ is considered in terms of an average $\overline{p0_i}$ and regions of low relative total pressure ($p0 < \overline{p0_i}$) and high relative total pressure ($p0 > \overline{p0_i}$). The extent parameter for a one-per-revolution pattern is defined as the circumferential extension of the low-pressure region [3], i.e. $\theta_i^- = \theta 2_i - \theta 1_i$. The circumferential distortion intensity for ring *i* is defined as:

(10) $$(\Delta P_C/P)_i = \left(\frac{\overline{p0_i} - \overline{p0_-}}{\overline{p0_i}}\right)_i$$

where

(11) $$\left(\overline{p0_-}\right)_i = \frac{1}{\theta_i^-}\int_{\theta 1_i}^{\theta 2_i} p0(\theta)_i \, \mathrm{d}\theta$$

The radial distortion intensity is calculated from the difference between the average total pressure of ring *i* and the average of the whole AIP:

(12) $$(\Delta P_R/P)_i = \frac{\overline{p0_{AIP}} - \overline{p0_i}}{\overline{p0_{AIP}}}$$

The total pressure recovery at the AIP is defined as an overall performance parameter:

(13) $$C_{dh} = \frac{\rho_{inf}(p0_{inf} - \overline{p0_{AIP}})}{W^2}$$

where ρ_{inf} is the freestream density, $p0_{inf}$ is the freestream total pressure and W is the intake mass-flow rate.

In addition to total pressure based parameters, some used parameters are based on the velocity field in the AIP. The distortion descriptor applied for swirl-based non-uniformities is considered in terms of the $SC60(\theta)$ parameter. It is defined as the ratio of $max\left(\left|\overline{V_{\theta 60}}\right|\right)$, the maximum absolute average circumferential velocity in a section of 60 deg (from a rotating rake), to the mean axial velocity $\overline{u_{AIP}}$:

(14) $$\mathrm{SC60}(\theta) = \frac{max(|\overline{V_{\theta 60}}|)}{\overline{u_{AIP}}}$$

The maximum value of the profile is defined as $SC60MAX$ and its related angle θ_{SCmax}. The swirl angle Φ is defined as the circumferential angle from the axial direction of the velocity vector and is considered positive in the clockwise direction looking at the AIP from downstream (i.e. pilot view):

(15) $$\Phi = \tan^{-1}\left(\frac{U_\theta}{U_x}\right)$$

It is noted that the velocity field in the AIP is obtained from the rotating flow directional probes test data by application of the calibration coefficients and several post-processing steps [12].

In order to investigate possible flow separation effects, the steady and unsteady static pressure distribution along the intake- lip and duct surfaces have also been obtained.

4.2. Full flight conditions

The tested full flight conditions are comprised of various aircraft speed, pressure altitude, angle of attack, sideslip angle, ambient temperature, rotor hub pitch, engine mass-flow rate and one rotor thrust settings, being representative for the full flight envelope.

Fig. 9 shows an example of the distribution of the total pressure in the AIP. The contour plot depicts the angular position (SAE convention) and AIP annulus walls. The total pressure is made dimensionless by normalizing against the free-stream total pressure. This eases comparison between different test conditions and allows interpretation of the total pressure loss. In general, it can be observed that the top sector shows two local areas with relatively low total pressure values.

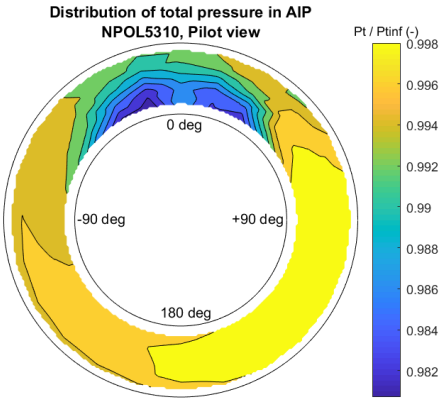

Fig. 9 Total pressure distribution in AIP for a VTOL condition

Fig. 10 shows an example of the distribution of the circumferential velocity in the AIP. In general, it can be observed that the top sector shows two local areas with relatively high circulation. The flow particles move circumferentially at radial outward located streamlines towards approx. 0 deg and then move at radial inward located streamlines from the approx. 0 deg plane away. Furthermore, it is stated that the swirl angle distribution is not always perfectly anti-symmetric (referred to the approx. 0 deg plane).

Presented at 47th European Rotorcraft Forum, United Kingdom, 7-9th September, 2021

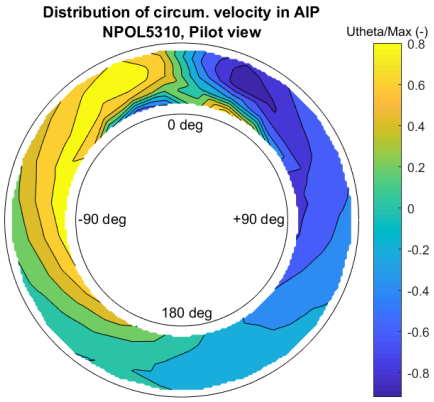

Fig. 10 Circumferential velocity distribution in AIP for a VTOL condition

Prior to generation of a database with distortion parameters $DC60(\theta)$ and $SC60(\theta)$, it has to be decided which value the sector scanning resolution should have. Analysis showed that a converged solution can be obtained if the sector scanning resolution is smaller than the step size of the rotating rake. It was decided to set the scanning resolution equal to 1 deg (the lowest used step size for the rotating rake is 7.5 deg). This results in plots with a typical staircase profile.

Fig. 11 shows an example of $DC60(\theta)$ and Fig. 12 of $SC60(\theta)$. In general, it can be observed that the total pressure distortion $DC60(\theta)$ has a single maximum at the top sector of the AIP. For the swirl distortion $SC60(\theta)$, however, two local maxima exist, in which the maximum is generally found at another angle than for the total pressure. This is related to the area weighing factor being larger for radially outward flow topologies, in combination with a slightly asymmetric absolute velocity field.

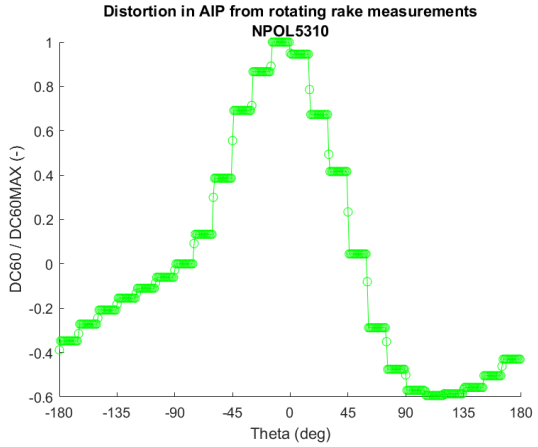

Fig. 11 DC60 profile for a VTOL condition

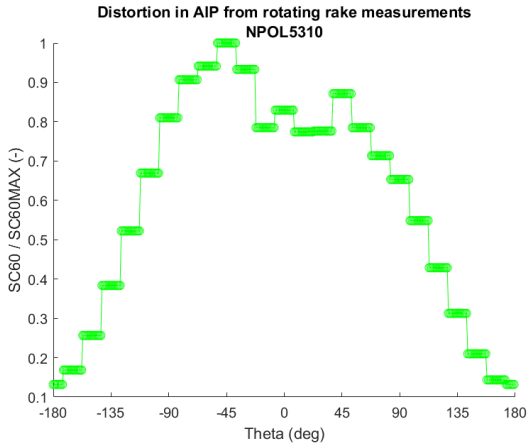

Fig. 12 SC60 profile for a VTOL condition

The $DC60MAX$ parameter allows for a first evaluation of the intake flow quality for the set of full flight conditions. It is found that only minor differences (within 0.03) exist in the averaged value for the AP mode, CM and VTOL subsets. Analysis of the distortion indices showed that the circumferential index CDI is in general much larger than the radial index RDI. Analysis of the radial distortion intensity $(\Delta P_R/P)_i$ revealed that the first two rings show positive values, while in good approximation the last three rings show negative values. The maximum absolute values are not related to a single flight mode. The circumferential distortion intensity $(\Delta P_C/P)_i$ showed that the largest components are found at the two inner rings.

Analysis of the $SC60MAX$ parameter showed that the largest values can be found for the AP mode. Comparison with the $DC60MAX$ parameter suggests that the swirl related parameter is not strongly correlated to the total pressure related parameter. This justifies the additional analysis based on the velocity distribution. In addition, it is stated that the largest values for the total pressure recovery C_{dh} are found for the VTOL mode, i.e. the averaged value for the AP or CM mode subset is approx. half of that for VTOL. As the distortion parameters are not showing such behaviour, additional analysis of the pressure distribution along the intake duct is required.

Therefore Fig. 13 shows the static pressure coefficient (Cp) distribution along the intake duct (in the symmetry plane) for an AP mode and VTOL mode. The axial development of the static pressure along the intake duct shows a negative gradient in front of the AIP for the top line and a positive gradient in front of the AIP for the bottom line. The positive gradient is related to a decelerating flow and in general can be considered to have a non-positive effect on the intake overall performance. However, for VTOL

Presented at 47th European Rotorcraft Forum, United Kingdom, 7-9th September, 2021

mode these gradients show much larger magnitudes compared to those of the AP mode. In addition, the duct Cp values for VTOL have much lower values compared to those of AP mode. The higher negative mean gradient for VTOL suggests that the relative large total pressure recovery can be explained by the relative large static pressure losses along the intake duct.

Fig. 14 shows the static pressure coefficient distribution along the intake lip (in the symmetry plane). It can be seen that for VTOL mode the bottom lip comprises a highly accelerated flow, while for the top lip a distinct suction peak can be observed. This does not hold for the AP mode, although the suction mass-flow rate for the considered AP mode is slightly higher than that for the considered VTOL mode.

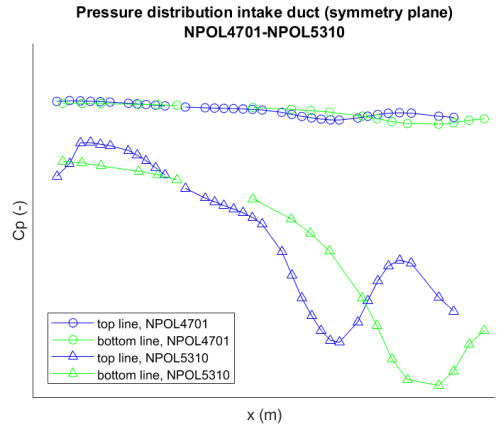

Fig. 13 Pressure distribution intake duct for an AP mode (NPOL4701) vs. VTOL mode (NPOL5310)

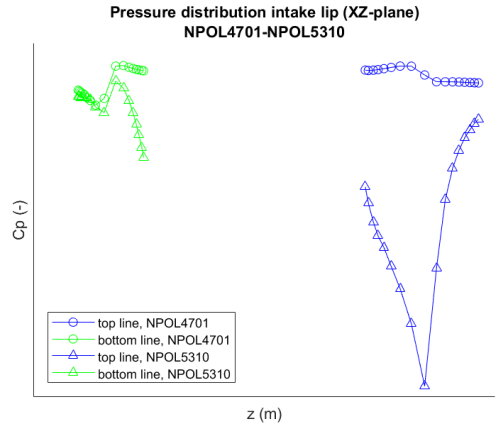

Fig. 14 Pressure distribution intake lip for an AP mode (NPOL4701) vs. VTOL mode (NPOL5310)

4.3. Sensitivity study

4.3.1. Effect of angle of attack variation

The database contains distortion parameters for a selected wide range of variations in angle of attack, sideslip angle, aileron deflection and mass-flow rate.

Consider the angle of attack to change from 0 to 10 deg. Then Fig. 15 shows that the pressure distribution on the wing is broadened and a suction peak is generated on the top surface near the leading edge (classical lifting surface). The horizontal axis depicts the relative chordwise position.

The sensitivity of key distortion parameters ($DC60MAX$, $max(\Delta P_R/P)_i$, $max(\Delta P_C/P)_i$) to angle of attack is obtained for AP, CM and VTOL conditions. It is found that the sensitivities largely behave linearly. As an example it is found that the sensitivity of $DC60MAX$ to angle of attack varies from -0.004 deg^{-1} (AP mode) to 0.001 deg^{-1} (VTOL mode). It is interesting to note that the data set for VTOL mode includes a variation in freestream velocity as well. This is due to the rotor induced velocity having a significant effect on both the angle of attack and WT speed for the VTOL mode, see Eqs. (3-4).

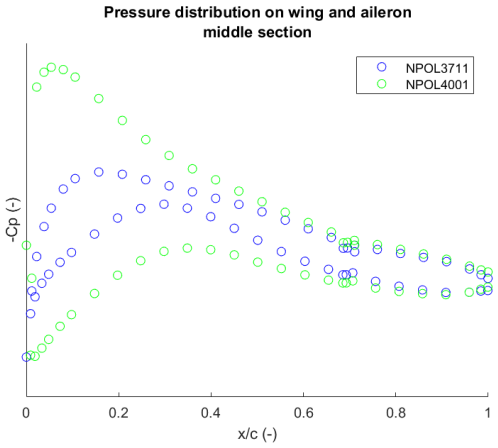

Fig. 15 Effect of angle of attack on wing pressure distribution for an AP mode (NPOL3711 = 0 deg, NPOL4001 = 10 deg)

4.3.2. Effect of sideslip angle variation

The sensitivity of key distortion parameters ($DC60MAX$, $max(\Delta P_R/P)_i$, $max(\Delta P_C/P)_i$) to sideslip angle is obtained for AP and VTOL conditions. As an example it is found that the sensitivity of $DC60MAX$ to sideslip angle varies from 0.001 deg^{-1} (AP mode) to -0.002 deg^{-1} (VTOL mode).

4.3.3. Effect of aileron deflection variation

The sensitivity of key distortion parameters ($DC60MAX$, $max(\Delta P_R/P)_i$, $max(\Delta P_C/P)_i$) to aileron deflection is obtained for AP conditions

Presented at 47th European Rotorcraft Forum, United Kingdom, 7-9th September, 2021

only. The sensitivity of $DC60MAX$ to aileron deflection is found to be negligible (i.e. less than 0.001 deg^{-1}). In addition, the expectation that the pressure distribution along the intake lip and duct is not significantly altered by aileron deflections was confirmed.

4.3.4. Effect of mass-flow rate variation

The sensitivity of key distortion parameters ($DC60MAX$, $max(\Delta P_R/P)_i$, $max(\Delta P_C/P)_i$) to mass-flow rate is obtained for AP, CM and VTOL conditions.

Fig. 16 shows that an increase in mass-flow results into an increase in distortion intensities. It is found in general that the circumferential intensity has a higher sensitivity to mass-flow than the radial intensity. In addition, the expectation that the pressure distribution on the wing is not significantly altered by variation of the suction mass-flow rate has been confirmed.

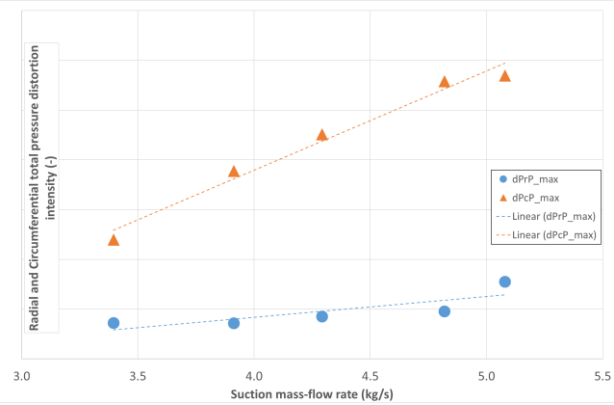

Fig. 16 Effect of mass-flow rate on distortion intensities for a VTOL mode

4.4. Unsteady pressures

The signals of the unsteady pressure sensors appeared to contain multiple peaks in the time domain (without overloads), which complicates spectral analysis in general. In order to analyze the flow unsteadiness, RMS values are obtained from the frequency domain, in which a filter has been applied for all test conditions (i.e. HPF = 10 Hz and LPF = 500 Hz). The RMS values in the AIP have been obtained from full rotating rake polars. In general, it can be observed that the largest RMS values in the AIP occur in the top sector, see the example in Fig. 17.

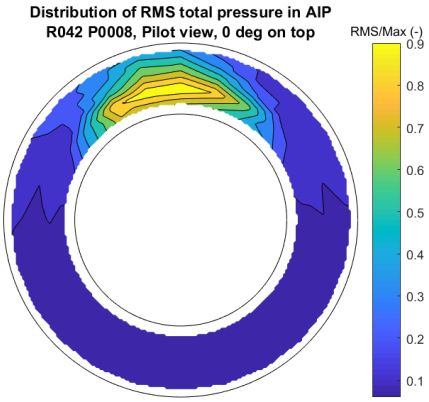

Fig. 17 Distribution of RMS total pressure in AIP

In order to investigate the development of unsteady pressures along the intake, 10 sensors have been mounted in the intake lip and duct surfaces (distributed over axial and angular positions). Fig. 18 shows an example of the RMS pressures (normalized by freestream dynamic pressure) along the intake duct for several AP mode conditions. The largest RMS values along the intake duct occur at the “cheeks”, i.e. side positions QI-09 and QI-10. This effect appears to be less clear for the VTOL cases, in which for some conditions the position QI-01 at the lip shows slightly larger RMS values. It is found that the largest dimensionless fluctuations occur for the VTOL conditions. The axial development of the fluctuations along the intake shows a positive gradient for AP- and CM modes, but a negative gradient for VTOL. It is also found that the ratio of maximum RMS value between AIP and duct varies between 5.3 and 15.5. Inspection of the test matrix suggests this to be correlated to the mass-flow rate (or Reynolds number at AIP).

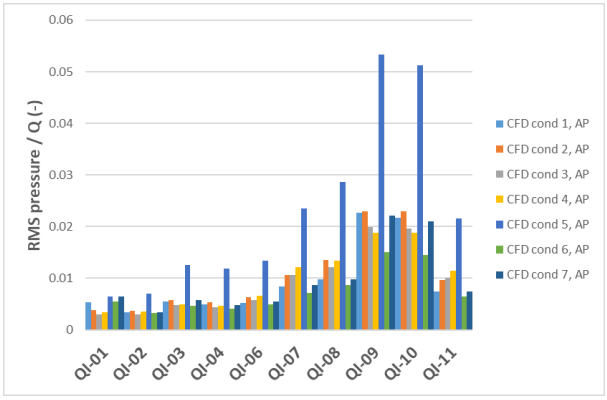

Fig. 18 Unsteady wall pressures in intake duct (AP mode)

Finally, some interesting observations were made during a brief sensitivity study. For AP mode, it is found that the RMS pressure distribution along the intake duct is not significantly altered by a

Presented at 47th European Rotorcraft Forum, United Kingdom, 7-9th September, 2021

variation in angle of attack or sideslip angle. However, an effect of mass-flow rate variation is observed; i) the RMS distribution along the intake is affected at the “cheek” positions in particular, ii) the area of maximum RMS value at the AIP remains at the same location but shows increased RMS value with increasing mass-flow rate. For VTOL mode, an effect of mass-flow rate variation is also observed; i) the negative axial gradient in RMS levels off (suggesting a reduction of the flow separation effect at the lip top area) and the RMS value at the intake “cheeks” increase significantly, ii) the area of maximum RMS value at the AIP remains at the same location but shows increased RMS value with increasing mass-flow rate.

5. CONCLUSIONS

A wind tunnel model has been successfully designed and manufactured for full-scale intake testing. A wind tunnel test has been successfully performed, simulating NGCTR full flight conditions and parameter variations. Analysis of the test data yields the following concluding statements for the basic intake performance.

The performance of an intake is strongly related to the flow quality at the AIP. It has been observed that the top sector of the AIP contains two local areas with relatively low total pressure values. The distortion parameter $DC60(\theta)$ has a single maximum at the top sector of the AIP. The velocity field in the AIP indicates two circulation zones (counter rotating vortices).

Conditions representing the full flight envelope have been tested.

- It can be observed that only minor differences (within 0.03) exist in $DC60MAX$ for the averaged value between AP, CM and VTOL modes.
- It is observed that the circumferential total pressure distortion index CDI is in general much larger than the radial total pressure distortion index RDI.
- The total pressure distortion intensities $max(\Delta P_R/P)_i$ and $max(\Delta P_C/P)_i$ are found to be each much less than a typical constraint of 2.5%.
- The total pressure recovery C_{dh} has the largest value for the VTOL mode, i.e. the averaged value for AP or CM mode is approx. half of that for VTOL. The axial development of the static pressure along the intake duct shows a negative gradient in front of the AIP for the top line and a positive gradient in front of the AIP for the bottom line. The positive gradient is related to a decelerating flow and in general can be considered to have a non-positive effect on the intake overall performance. For VTOL mode these gradients show much larger magnitudes compared to those of the AP mode. The higher negative mean gradient for VTOL suggests that the relative large total pressure recovery can be explained by the relative large static pressure losses along the intake duct.
- The intake lip suffers from fixed suction peaks. For AP and CM modes a suction peak can be found at the bottom lip, while for VTOL mode a suction peak occurs at the top lip.

The sensitivity of key distortion parameters to variation of angle of attack, sideslip angle, aileron deflection and mass-flow rate has been investigated.

- Variations of the angles yield a maximum absolute sensitivity in $DC60MAX$ of 2% / deg (CM) and less than 1% / deg (AP, VTOL). For $max(\Delta P_R/P)_i$ and $max(\Delta P_C/P)_i$ a common maximum value of 6E-5 / deg is found.
- The effect of increasing mass-flow rate is a steepening of the axial pressure coefficient gradient, thus improving the mean flow acceleration towards the AIP. However, increasing mass-flow rate always yields increased values of the considered distortion parameters. The maximum sensitivity in $DC60MAX$ is 2% / (kg/s). For $max(\Delta P_R/P)_i$ it is 0.1% / (kg/s) and for $max(\Delta P_C/P)_i$ it is 0.4% / (kg/s).
- The expectation that the pressure distribution on the wing is not significantly altered by variation of the suction mass-flow rate has been confirmed.

The basic intake suffers from a relative high level of flow unsteadiness, which can be associated to flow separation (the model is not equipped with a rotor).

- The time signals of wall static pressures and AIP total pressures contain multiple peaks, which complicate spectral analysis. It has been observed that the largest RMS values in the AIP occur in the top sector.
- The axial development of the static pressure fluctuations along the intake shows a positive gradient for AP- and CM modes, but a negative gradient for VTOL. The largest RMS values along the intake duct occur at the “cheeks”. This effect is less clear for the VTOL cases, in which

Presented at 47th European Rotorcraft Forum, United Kingdom, 7-9th September, 2021

for some conditions the lip top area shows slightly larger RMS values. In general, it has been observed that the largest dimensionless fluctuations occur for the VTOL conditions.

- Variation of model attitude at AP mode does not significantly alter the RMS distribution along the intake duct. Increasing the mass-flow rate affects the RMS values at the intake "cheeks" in particular (increased RMS). The area of maximum flow unsteadiness in the AIP remains at the same location but obtains an increased RMS value as well.

6. ACKNOWLEDGEMENTS

This work was performed as part of the project TRINIDAT and has received funding from the Clean Sky 2 Joint Undertaking (JU) under grant agreement No 831810. The JU receives support from the European Union's Horizon 2020 research and innovation programme and the Clean Sky 2 JU members other than the Union.

This paper reflects only the author's view; the JU is not responsible for any use made of the information contained herein.

7. REFERENCES

[1] Horizon 2020, Clean Sky 2, Fast Rotorcraft IADP, https://www.cleansky.eu/fast-rotorcraft-iadp

[2] Horizon 2020, Clean Sky 2, TRINIDAT project, GA no. 831810, https://project.nlr.nl/trinidat

[3] SAE-ARP1420 C: Gas Turbine Engine Inlet Flow Distortion Guidelines, Rev. C. April 2017.

[4] G. Gibertini, A. Zanotti, G. Campanardi, F. Auteri, D. Zagaglia, G. Crosta: Wind-tunnel tests of the ERICA tiltrotor optimised air-intake, The Aeronautical Journal, May 2018, Volume 122, No 1251, May 2018.

[5] N. S. Payne: New Large-Scale Model inlet Performance Testing Capability for the AEDC PWT 16 T/S Wind Tunnels, AIAA Aviation Forum, June 25-29, 2018, Atlanta, Georgia, 2018 Aerodynamic Measurement technology and Ground testing Conference.

[6] J. G. Leishman: Principles of helicopter aerodynamics, Cambridge University Press,2000. Section 2.4 Momentum Analysis in Forward Flight.

[7] D.G. MacManus, N. Chiereghin, D. G. Prieto, P. Zachos: Complex Aeroengine Intake Ducts and Dynamic Distortion, AIAA Journal, Vol. 55, No. 7, July 2017.

[8] AGARDograph 109, Subsonic wind tunnel wall corrections, October 1966.

[9] AGARDograph 336, Wind tunnel wall corrections, October 1998.

[10] Labrujère, Th.E., Correction for wall interference by means of a measured-boundary-condition method, NLR TR 84114 U, 1984.

[11] Labrujère, Th.E., Maarsingh, R.A. and Smith, J., Evaluation of measured-boundary-condition methods for 3D subsonic wall interference, NLR TR 88072 U, 1988.

[12] A.C. de Bruin and J. van Muijden, Review of flow field measurement technique with 5-hole rake, NLR-TR-2009-501, NLR, May 2011.

[13] E. Norde, S. van 't Hoff, H. van der Ven, E. van der Weide, F. Spek, Icing characteristics on NGCTR engine inlet for relevant certification conditions, 47th ERF, paper 48, 2021.